


 Cite this: *RSC Adv.*, 2021, 11, 34095

Photoluminescence properties of cuprous phosphide prepared through phosphating copper with a native oxide layer†

 Xue Peng,^a Yanfei Lv,^{*a} Li Fu,^a Fei Chen,^{id}^a Weitao Su,^a Jingzhou Li,^{*b} Qi Zhang^a and Shichao Zhao^{id}^{*a}

 Received 23rd September 2021
 Accepted 14th October 2021

DOI: 10.1039/d1ra07112b

rsc.li/rsc-advances

Although cuprous phosphide (Cu₃P) has been widely studied and applied in other fields, its photoluminescence (PL) properties are rarely investigated. Herein, we report that Cu₃P can emit near-infrared light at 750 nm. We show that the annealing and the presence of cuprous oxide can enhance the PL emission. The mechanism of the PL enhancement is the improvement of crystal quality and the formation of a space charge region. Our results provide a reference for improving the PL properties of p-type semiconductors.

1. Introduction

Near-infrared light has important applications in various fields, such as communication, sensing, physics, chemistry and biology.^{1–9} For example, the infrared window of biological tissue is 700–900 nm, and the near-infrared light within this range can be used to detect blood oxygen signals.^{10,11} Cuprous phosphide (Cu₃P) is widely used in catalysts, electrode materials and welding materials. However, as a p-type semiconductor material, its electrical and optical properties and applications have been neglected.^{12–19} Mu *et al.* synthesized self-doped colloidal copper phosphide (Cu_{3–x}P) nanocrystals in solution using a “one-pot method” and found that Cu_{3–x}P emitted fluorescence at 550–650 nm.²⁰ The above reports indicate that Cu_{3–x}P is a kind of fluorescent material, which has potential uses in fluorescence emission and photodetectors.²¹ However, the fluorescence emission wavelength they reported is in the visible light range, which is different from other researchers' results. Fu *et al.* reported that the band gap of Cu₃P is 1.55 eV (in the range of infrared).²² Therefore, the fluorescence emission wavelength of Cu₃P needs further study. In addition, the reported fluorescence emission intensity is low, so how to improve the intensity is also a scientific problem that needs to be studied.

Herein, we prepared the Cu₃P through phosphating process and studied its photoluminescence properties in detail. We

observed that the presence of cuprous oxide and annealing enhanced the fluorescence emission of Cu₃P. We proposed that the mechanism of the PL enhancement is due to the band bending and the trapped carriers in the space charge region formed between cuprous phosphide and cuprous oxide. Our study provides a reference method for improving the fluorescence properties of Cu₃P, which is useful for the optoelectronic applications.

2. Experimental

2.1. Preparation of cuprous phosphide film

Cuprous phosphide was prepared by a chemical reaction method.²³ Sodium hypophosphite and copper with a native oxide layer were used as precursors. Sodium hypophosphite (0.05 mol) was loaded into a corundum crucible. The copper foil (1 cm × 1 cm) was put on the corundum crucible. Then the corundum crucible with precursors was placed into the corundum tube and pumped with argon as a protective gas for 20 min, and then the tube was sealed at one bar pressure. After that, the corundum tube was heated to 300 °C with a heating rate of 10 °C min^{−1} and held at 300 °C for 2 h. After that, the corundum tube was naturally cooled to room temperature to obtain Cu₃P. During the cooling process, the residual gas in the tube was discharged into the hazardous gas treatment system. To study the effect of annealing on the crystallization and optical properties, cuprous phosphide was heated at 400, 500, 600, 700 and 800 °C for 2 h, respectively, under argon.

2.2. Acid treatment of cuprous phosphide

To investigate the effect of the presence of cuprous oxide (Cu₂O) on the optical properties of Cu₃P, the Cu₃P sample containing Cu₂O was treated in acid solution to remove Cu₂O. The cuprous

^aCollege of Materials & Environmental Engineering, Hangzhou Dianzi University, Hangzhou, 310018, P. R. China. E-mail: lvyanyanfei@hdu.edu.cn; zhaoshichao@hdu.edu.cn

^bHangzhou Institute for Advanced Study, University of Chinese Academy of Sciences, Hangzhou, 310024, P. R. China. E-mail: lijingzhou@ucas.ac.cn

† Electronic supplementary information (ESI) available. See DOI: 10.1039/d1ra07112b



phosphide annealed at 400 °C was immersed in a dilute hydrochloric acid (0.5 mol L⁻¹) solution for 60 min, then cleaned with de-ionized water and dried in the air.

2.3. Characterization

The crystal structure was conducted on an X-ray diffractometer (XRD, Thermo ARLXTRA). The surface morphology and elementary composition were analyzed on a field emission scanning electron microscopy (FSEM, FEI Apero S). Raman spectrum was performed on an HR Evo Nano (HORIBA) with a 532 nm laser. The diffuse reflectance ultraviolet visible spectrum (UV-vis DRS) was carried on a Shimadzu UV-3600. The photoluminescence spectrum (PL) was collected in an HR Evo Nano (HORIBA). The conductive type of cuprous phosphide was characterized by a hot-probe method. During the test, the hot probe connects to the positive terminal and the cold probe to the negative terminal. The voltage was measured using a Keysight 34461A digit multimeter. The probe was heated by a hot metal bar.

3. Results and discussion

3.1. SEM and EDX

Surface morphology and elemental mapping of Cu₃P film are shown in Fig. 1. The film is composed of crystalline particles. Typical thickness of the film is *ca.* 2.7 μm (Fig. S1†). With the increase of heating temperature, the average particle size

increased from 250 ± 20 nm for the sample annealed at 300 °C (Fig. 1a) to 500 ± 20 nm for the sample at 700 °C (Fig. 1e). This indicates that the Cu₃P crystals were undergoing recrystallization during the annealing process, resulting the improved crystalline quality. Different from other samples, the one treated at 800 °C (Fig. 1f) shows more continuous and smoother surface, which is due to the formation of eutectic mixture of copper (from an excess of unreacted copper substrate) and Cu₃P.²⁴ To obtain the composition of the Cu₃P sample annealed at 400 °C, we randomly tested the energy dispersive X-ray spectrum (EDX), shown in Fig. 1g-i. Copper and P elements are relatively evenly distributed in the test area, while oxygen is localized in some areas. This indicates that Cu₃P contains a certain amount of copper oxides. The oxygen comes from the native oxide layer of copper precursor. The elemental ratios of Cu : P : O in Cu₃P samples grown at 300 °C and heat treated at 400, 500, 600, 700 and 800 °C are *ca.* 5 : 2 : 3, 4 : 1 : 5, 4 : 2 : 4, 4 : 3 : 3, 5 : 2 : 3, and 4 : 2 : 4, respectively (Table 1). The atomic ratio is not constant, nor does it show regularity with annealing temperature, which is due to the inhomogeneity of the sample and the error of the EDX.

3.2. XRD

Fig. 2 is the XRD pattern of Cu₃P annealed at different temperatures. The peaks without marks are corresponding to the diffraction peak of Cu₃P (PDF # 71-2261).²⁵ The peaks at 43.19°, 50.29°, 73.88° and 89.61° are derived from copper

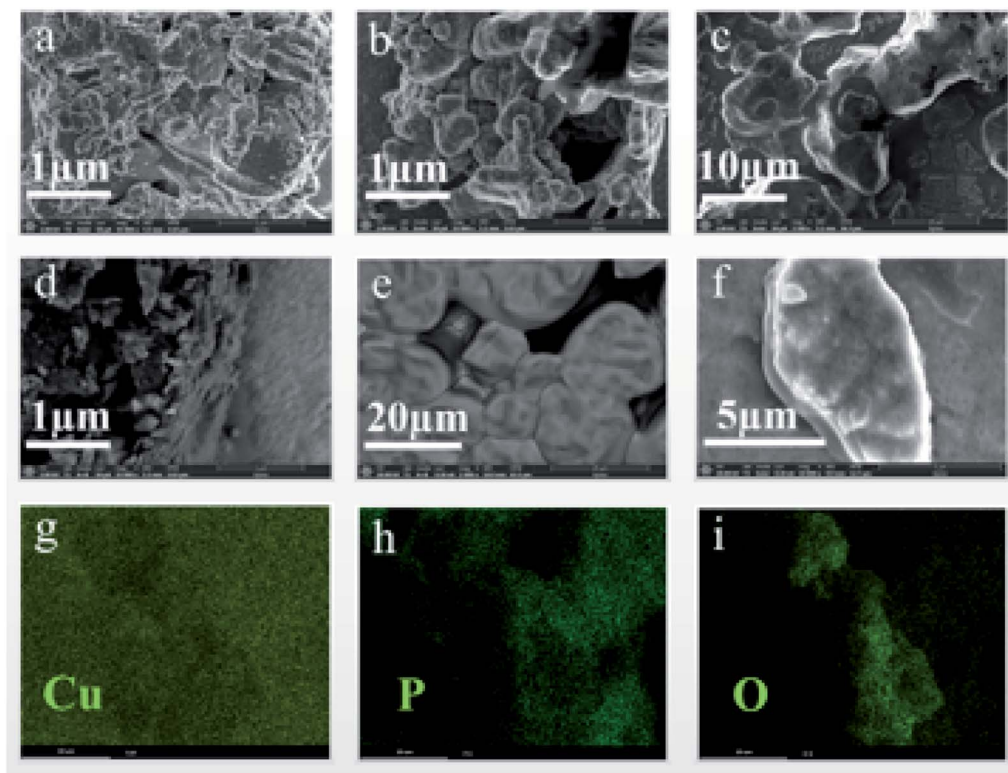


Fig. 1 SEM and EDX images of Cu₃P. (a), (b), (c), (d), (e) and (f) are the SEM images of the samples grown at 300 °C and the samples heat treated at 400, 500, 600, 700 and 800 °C, respectively; (g), (h) and (i) are the distribution diagrams of Cu, P and O elements of Cu₃P, respectively, corresponding to the sample heated at 400 °C.



Table 1 The atomic ratio (atm%) of Cu, P and O elements in Cu₃P before and after annealing. The growth temperature is 300 °C, and the annealing temperature is 400 °C, 500 °C, 600 °C, 700 °C and 800 °C, respectively

Temperature (°C)	300	400	500
Cu : P : O (atm%)	51.1 : 21.8 : 27.1	41.2 : 11.6 : 47.2	40.8 : 19.2 : 40.0
Temperature (°C)	600	700	800
Cu : P : O (atm%)	41.0 : 27.7 : 36.3	49.2 : 23.6 : 27.2	38.2 : 16.5 : 45.3

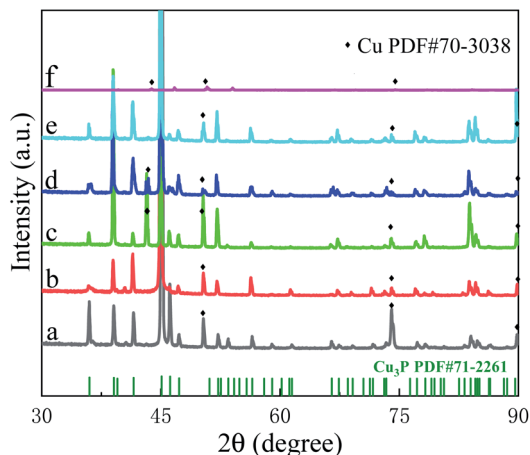


Fig. 2 XRD of Cu₃P before and after annealing: (a) grown at 300 °C without annealing; annealed at (b) 400, (c) 500, (d) 600, (e) 700 and (f) 800 °C. The reference peaks of Cu₃P are corresponding to PDF#71-2261.

(PDF#70-3038), which comes from the excess copper precursor beneath the Cu₃P. The XRD spectra are dominated by the Cu₃P diffraction peaks, indicating the main component of the sample is Cu₃P. As the temperature increases from 300 °C to 700 °C, the peak intensity of Cu₃P changes. For example, the peak at increases 50.29° and 73.88° and decreases at 89.61°, indicating that the recrystallization process takes place and the crystallization quality improved in the process of annealing. When the temperature reaches 800 °C, the diffraction peak changes greatly: only a few diffraction peaks (47.29°, 54.09°, 84.56°) are observed according to Fig. 2f and the intensity of copper peaks increases relative to Cu₃P, which are resulted from the forming of eutectic mixture. The peak position of Cu₃P does not change with the annealing temperature, indicating that there is no stress inside the Cu₃P crystal. Unlike the copper oxides observed by EDX data, XRD does not, which indicates that the amount of copper oxides is too low or the crystallinity is too poor for XRD.

3.3. Raman

In order to further analyze the composition of the sample, we performed Raman spectroscopy. Fig. 3 shows the Raman spectra of Cu₃P before and after annealing. The peaks centered at 273 cm⁻¹ and 607 cm⁻¹ are due to Cu₃P,²⁶ and the peak at 323 cm⁻¹ is derived from cuprous oxide (Cu₂O).²⁷ The peak intensity of Cu₃P is stronger than that of Cu₂O, indicating that the main component of the sample is Cu₃P combined with small amount of Cu₂O. In addition, we observe that annealing

has no obvious effect on the Raman peak position and peak shape, consisting with the analysis results of XRD, indicating that there is no stress in the crystal.

3.4. UV-vis

Fig. 4a is a typical UV-vis DRS of Cu₃P. Cuprous phosphide is better at absorbing short wavelengths (less than 400 nm) than long wavelengths (from 400 nm to near-infrared light). We can find two absorption edges, located at 400–475 nm and 680–740 nm, respectively. The former is due to the absorption of Cu₂O, and the latter corresponds to the absorption of Cu₃P.

In order to obtain the optical band gap width of Cu₃P, we processed UV-vis DRS data. Firstly, we converted UV-vis DRS data into absorption spectrum, then, plotted it with photon energy E as horizontal coordinate axis, and $(\alpha h\nu)^2$ as the vertical coordinate axis, as shown in Fig. 4b and c.^{28–30} The horizontal ordinate of the point where the extension line of the linear part of the curve intersects with the longitudinal coordinate equal to zero is the value of the band gap width. The band gaps of Cu₃P and Cu₂O are 1.67 eV and 2.43 eV, respectively, which are consistent with the results of other groups.^{22,31–34}

3.5. PL

Fig. 5 shows the normalized PL spectra of Cu₃P before and after annealing. The spectra were fitted by a Gaussian function. Detailed data obtained by fitting are listed in Table 2. We find a broad peak ranging from 500 to 800 nm in the sample before annealing (Fig. 5a). The peak can be fitted into three subpeaks, centered at 631.4 nm, 734.2 nm and 796.3 nm, respectively. We

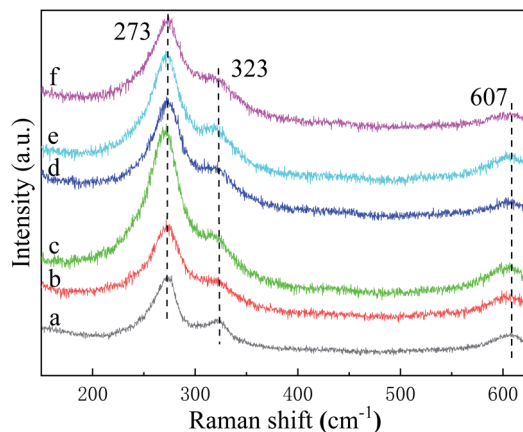


Fig. 3 Raman spectra of Cu₃P before and after annealing: (a) grown at 300 °C without annealing; annealed at (b) 400, (c) 500, (d) 600, (e) 700 and (f) 800 °C, respectively.



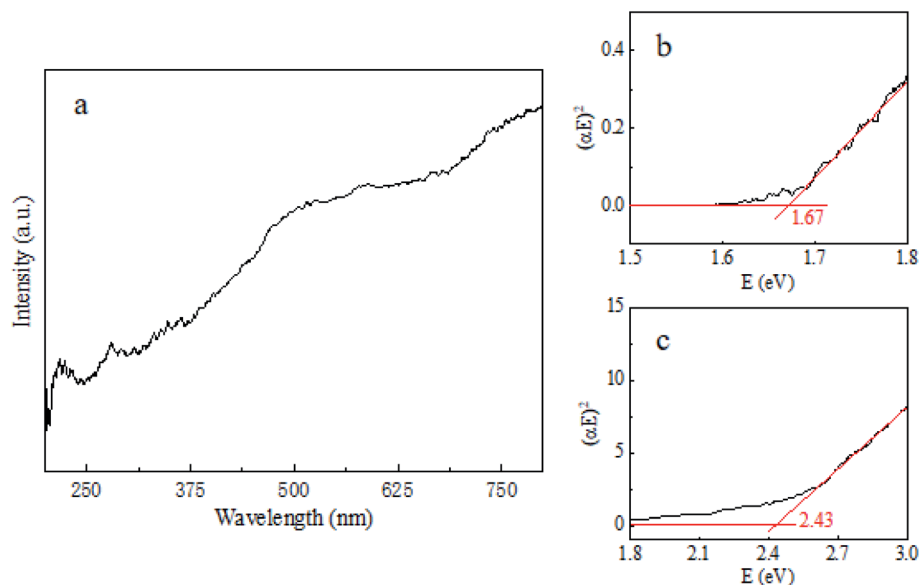


Fig. 4 Typical UV-vis diffuse reflection spectrum of Cu_3P (containing cuprous oxide) (a). Tauc plot for Cu_3P (b) and Cu_2O (c) composites.

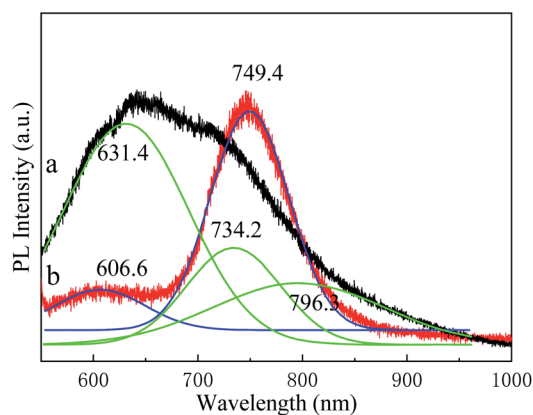


Fig. 5 Photoluminescence spectra of Cu_3P grown at 300 °C (a) and annealed at 400 °C (b). The black and red curves are experimental data, while the green and blue curves are fitted curves by Gaussian function.

speculate that the peak at 631.4 nm is from the band-edge fluorescence emission of Cu_2O , the peak at 734.2 nm from Cu_3P , and the peak at 796.3 nm from the impurity level emission of Cu_3P .^{12,35} In addition, the PL intensity of Cu_3P is weaker than that of Cu_2O . After annealing, the peak of Cu_2O blueshifts to 606.6 nm, and the peak of Cu_3P redshifts to 749.4 nm, and

the peak at 796.3 nm disappears. The shifts of the peak should be related to the improvement of the crystal quality and grain boundary. The PL emission of Cu_3P is greatly enhanced, while that of Cu_2O is sharply reduced. The PL intensity ratio of Cu_3P to Cu_2O is increased from 71% before annealing to 500% after annealing. In addition, the full width at half maximum (FWHM) of Cu_3P decreases obviously after annealing. Our observation indicates that the annealing can greatly improve the fluorescence properties of Cu_3P . We found that the optimal annealing temperature is 400 °C. When the annealing temperature rises to 600 °C and 700 °C, the PL intensity of Cu_3P relative to Cu_2O decreases, as shown in Fig. S2.† When the temperature reaches 800 °C, the PL of Cu_3P is hardly even observed. We believe the annealing at higher temperature decreases crystalline quality. The Cu_3P may be partially decomposed or oxidized by residual oxygen in the annealing system.

There are two reasons for the fluorescence enhancement of Cu_3P by annealing: improvement of the crystal quality and existence of a space charge region.^{36–38} First, annealing improves the crystallization quality and reduces the impurity level, enhancing the interband emission. Secondly, annealing improves the bonding quality between Cu_3P and Cu_2O grain interfaces. The conductive type of Cu_3P was determined by hot-probe method. Hot-probe characteristic for Cu_3P is shown in Fig. S3.† The data show measured voltages are depended on the

Table 2 Detailed fitting data of PL spectra of Cu_3P grown at 300 °C and annealed at 400 °C, corresponding to the data in Fig. 5

Sample	Grown at 300 °C			Annealed at 400 °C	
Peak position (nm)	631.4	734.2	796.3	606.6	749.4
Assignment	Cu_2O	Cu_3P	Defects of Cu_3P	Cu_2O	Traps in Cu_3P
Peak intensity (peak integral area)	124.9	41.0	47.5	16.3	77.6
Full width at half maximum (FWHM)	120.0	90.2	163.8	85.8	75.4



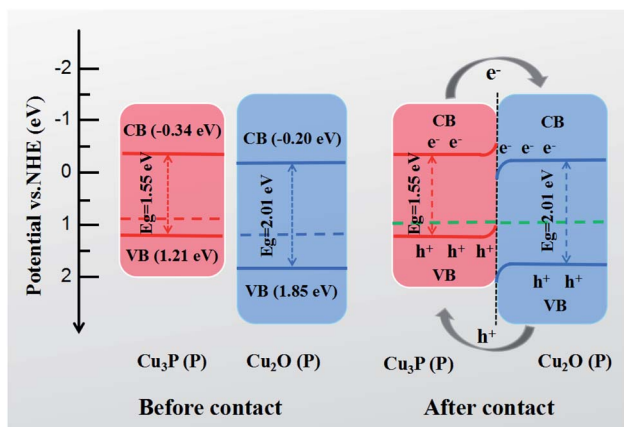


Fig. 6 Schematic diagram of photogenerated carrier transfer mechanism between Cu_3P and Cu_2O . See references for the energy level data.^{22,40} CB, VB, P, e^- , h^+ represent conduction band, valence band, p-type, electron and hole, respectively.

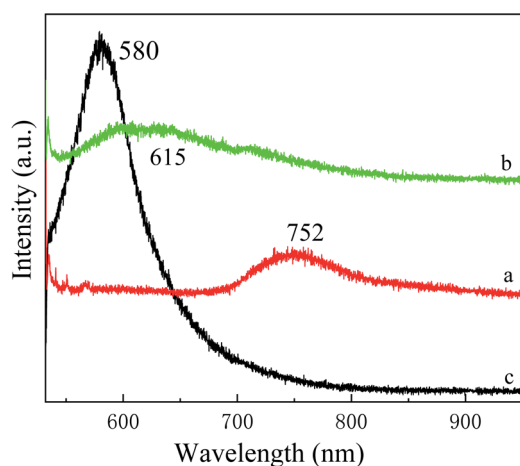


Fig. 7 Fluorescence spectra of Cu_3P before (a) and after (b) hydrochloric acid treatment. Curve (c) is the fluorescence spectrum of Cu_2O . The Cu_3P sample was grown at 300°C and annealed at 400°C .

heating time. Cu_3P is of p-type as negative values of measured voltages are observed under hot status.³⁹ Both Cu_3P and Cu_2O are p-type semiconductors. The band gap width of Cu_2O is larger than that of Cu_3P . The conduction band energy level of Cu_2O is slightly higher than that of Cu_3P , and the valence band energy level of Cu_2O is lower than that of the Cu_3P , shown in Fig. 6a.²² Therefore, the hole transfer from Cu_2O to Cu_3P occurs and forms a space charge region at the interface when the two materials come into contact, shown in Fig. 6b. The space charge region leads to energy band bending upwards at the side of Cu_3P and down at the side of Cu_2O . The band energy levels stagger at the junction of the two materials to form carrier traps. The trap accumulates the photogenerated electrons and holes in the space charge region at the side of Cu_3P , which enhance the near-infrared light emission of Cu_3P .

In order to verify the space charge region mechanism, we use hydrochloric acid to remove Cu_2O partially to destroy the space

charge region. If the space charge region were destroyed, the transfer channel of the photogenerated carrier is cut off, then the PL intensity of Cu_3P should be decreased. The experimental results are shown in Fig. 7. We find the PL intensity of Cu_3P decreases, and that of Cu_2O increases. The results agree with our hypothesis, so our proposed mechanism is correct.

4. Conclusion

In this paper, the fluorescence properties of Cu_3P were studied. Cuprous phosphide emitted near-infrared emission under the excitation of short wavelength light. The PL of Cu_3P was affected by annealing and the presence of Cu_2O . Annealing improved the crystal quality and the fluorescence property. Cuprous oxide enhanced the PL emission through the formation of space charge region. Our results show that the method of forming hole traps in p-type semiconductor can help us to obtain efficient fluorescence emission materials through energy band engineering.

Author contributions

Yanfei Lv, Li Fu, Fei Chen, Qi Zhang conceived and designed the experiments; Xue Peng and Weitao Su performed the experiments; Xue Peng prepared the manuscript; Jingzhou Li and Shichao Zhao performed the data analyses and wrote the paper.

Conflicts of interest

There are no conflicts to declare.

References

- M. T. Hasan, B. H. Lee, C. W. Lin, A. McDonald-Boyer, R. Gonzalez-Rodriguez, S. Vasireddy, U. Tsedev, J. Coffey, A. M. Belcher and A. V. Naumov, *2d Mater*, 2021, **8**, 035013.
- S. C. Park, W. S. Yang, J. Y. Ahn, J. B. Park, J. H. Lee, Y. Jung, H. R. Kim, J. Y. Kim, J. M. Lim and B. H. Hong, *2d Mater*, 2021, **8**, 035012.
- T. Horimoto, N. Kannari and K. Sato, *Appl. Surf. Sci.*, 2021, **558**, 149841.
- L. Liu, R. Z. Li, L. Z. Zhang, P. Zhang, G. D. Zhang, S. Q. Xia and X. T. Tao, *J. Alloys Compd.*, 2021, **874**, 159943.
- J. Qian, Y. L. Luan, M. S. Kim, K. M. Ho, Y. Shi, C. Z. Wang, Y. Li and Z. Fei, *Phys. Rev. B*, 2021, **103**, L201407.
- Z. C. Guo, X. R. Liu, H. Y. Yu, F. J. Hou, S. M. Gao, L. L. Zhong, H. Xu, Y. Yu, J. L. Meng and R. R. Wang, *Spectrochim. Acta, Part A*, 2021, **257**, 119774.
- W. Y. Ma, S. L. Yu and T. G. Zhao, *Opt. Commun.*, 2021, **493**, 127037.
- J. W. John, V. Dhyani, S. Singh, A. Jakhar, A. Sarkar, S. Das and S. K. Ray, *Nanotechnology*, 2021, **32**, 315205.
- T. T. P. Hoang, V. D. Pham and T. Son, *J. Nanosci. Nanotechnol.*, 2021, **21**, 5535–5541.
- S. A. Manea, M. L. Vlad, D. Rebleanu, A. G. Lazar, I. M. Fenyo, M. Calin, M. Simionescu and A. Manea, *Oxid. Med. Cell. Longevity*, 2021, **2021**, 6685612.



- 11 W. X. Liu, L. D. Xing, L. Y. Yao, Z. H. Zou and Y. Zhang, *Zhongguo Yi Liao Qi Xie Za Zhi*, 2021, **45**, 280–283.
- 12 S. X. Hua, D. Qu, L. An, W. S. Jiang, Y. J. Wen, X. Y. Wang and Z. C. Sun, *Appl. Catal., B*, 2019, **240**, 253–261.
- 13 P. He, J. C. Feng and H. Zhou, *J. Mater. Sci. Technol.*, 2005, **21**, 493–498.
- 14 X. P. Xu, Q. J. Ma and C. Z. Xia, *High Temp. Mater. Processes*, 2019, **38**, 651–661.
- 15 N. A. M. Zahri, F. Yusof, T. Ariga, A. S. M. A. Haseeb, M. A. Mansoor and N. L. Sukiman, *Mater. Sci. Technol.*, 2019, **35**, 2004–2012.
- 16 A. Wolff, T. Doert, J. Hunger, M. Kaiser, J. Pallmann, R. Reinhold, S. Yogendra, L. Giebeler, J. Sichelschmidt, W. Schnelle, R. Whiteside, H. Q. N. Gunaratne, P. Nockemann, J. J. Weigand, E. Brunner and M. Ruck, *Chem. Mater.*, 2018, **30**, 7111–7123.
- 17 X. D. Zhang, J. Yan and L. Y. S. Lee, *Appl. Catal., B*, 2021, **283**, 119624.
- 18 B. A. Tappan, K. Y. Chen, H. P. Lu, S. M. Sharada and R. L. Brutchey, *ACS Appl. Mater. Interfaces*, 2020, **12**, 16394–16401.
- 19 L. De Trizio, R. Gaspari, G. Bertoni, I. Kriegel, L. Moretti, F. Scotognella, L. Maserati, Y. Zhang, G. C. Messina, M. Prato, S. Marras, A. Cavalli and L. Manna, *Chem. Mater.*, 2015, **27**, 1120–1128.
- 20 H. R. Mu, Z. K. Liu, X. Z. Bao, Z. C. Wan, G. Y. Liu, X. P. Li, H. Y. Shao, G. C. Xing, B. Shabbir, L. Li, T. Sun, S. J. Li, W. L. Ma and Q. L. Bao, *Front. Optoelectron.*, 2020, **13**, 139–148.
- 21 T. Sun, Y. J. Wang, W. Z. Yu, Y. S. Wang, Z. G. Dai, Z. K. Liu, B. N. Shivananju, Y. P. Zhang, K. Fu, B. Shabbir, W. L. Ma, S. J. Li and Q. L. Bao, *Small*, 2017, **13**(42), 1701881.
- 22 Z. Y. Fu, X. Y. Ma, B. Xia, X. Y. Hu, J. Fan and E. Z. Liu, *Int. J. Hydrogen Energy*, 2021, **46**, 19373–19384.
- 23 Y. Zuo, J. Shen, Y. D. Hu and R. H. Gao, *J. Mater. Process. Technol.*, 2018, **253**, 27–33.
- 24 T. Noda, K. Oikawa, S. Itoh, M. Hino and T. Nagasaka, *Calphad*, 2009, **33**, 557–560.
- 25 J. Lin, C. H. Zeng, X. M. Lin, C. Xu and C. Y. Su, *Adv. Sci.*, 2020, **7**(14), 2000736.
- 26 S. L. Liu, X. D. He, J. P. Zhu, L. Q. Xu and J. B. Tong, *Sci. Rep.*, 2016, **6**, 35189.
- 27 B. Houn, J. K. Wu, P. C. Yeh, W. L. Yeh and C. K. Sun, *J. Electroceram.*, 2021, **45**(3), 129–134.
- 28 E. A. Davis and N. F. Mott, *Philosophical Magazine*, 1970, **22**, 0903–0922.
- 29 J. Tauc, R. Grigorovici and A. Vancu, *Phys. Status Solidi B*, 1966, **15**, 627–637.
- 30 F. P. Yan, F. G. Yang, H. Zhang and P. H. Luo, *Mater. Res. Express*, 2021, **8**(4), 045508.
- 31 R. Gaspari, F. Labat, L. Manna, C. Adamo and A. Cavalli, *Theor. Chem. Acc.*, 2016, **135**(3), 73.
- 32 T. Begildayeva, S. J. Lee, Y. Yu, J. Park, T. H. Kim, J. Theerthagiri, A. Ahn, H. J. Jung and M. Y. Choi, *J. Hazard. Mater.*, 2021, **409**, 124412.
- 33 A. A. Dubale, C. J. Pan, A. G. Tamirat, H. M. Chen, W. N. Su, C. H. Chen, J. Rick, D. W. Ayele, B. A. Aragaw, J. F. Lee, Y. W. Yang and B. J. Hwang, *J. Mater. Chem. A*, 2015, **3**, 12482–12499.
- 34 M. A. Hossain, R. Al-Gaashani, H. Hamoudi, M. J. Al Marri, I. A. Hussein, A. Belaidi, B. A. Merzougui, F. H. Alharbi and N. Tabet, *Mater. Sci. Semicond. Process.*, 2017, **63**, 203–211.
- 35 T. Wu, H. Zheng, Y. C. Kou, X. Y. Su, N. R. Kadasala, M. Gao, L. Chen, D. L. Han, Y. Liu and J. H. Yang, *Microsyst. Nanoeng.*, 2021, **7**(1), 23.
- 36 L. Y. Zhang, F. Q. Wang, S. Wang, H. W. Huang, X. M. Meng, Y. R. Ouyang, W. Y. Yuan, C. X. Guo and C. M. Li, *Adv. Funct. Mater.*, 2020, **30**(43), 2003933.
- 37 F. Q. Wang, S. Wang, D. B. Wu, H. W. Huang, W. Y. Yuan and L. Y. Zhang, *Appl. Surf. Sci.*, 2021, **537**, 147860.
- 38 Y. Y. Gong, X. H. Liu, Y. Y. Gong, D. B. Wu, B. H. Xu, L. Bi, L. Y. Zhang and X. S. Zhao, *J. Colloid Interface Sci.*, 2018, **530**, 189–195.
- 39 G. Golan, A. Axelevitch, B. Gorenstein and V. Manevych, *Microelectron. J.*, 2006, **37**, 910–915.
- 40 J. Singh, S. Juneja, R. K. Soni and J. Bhattacharya, *J. Colloid Interface Sci.*, 2021, **590**, 60–71.

